Research Article

For reprint orders, please contact: reprints@futuremedicine.com

Nanomedicine

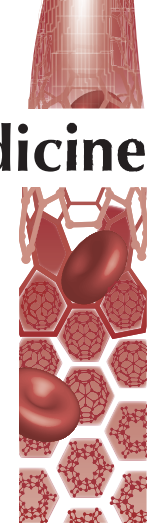

HA/PEI-coated acridine orange-loaded gold-core silica shell nanorods for cancer-targeted photothermal and chemotherapy

Carolina F Rodrigues[1], Natanael Fernandes[1], Duarte de Melo-Diogo[1], Paula Ferreira[2], Ilídio J Correia*,[1,2] & André F Moreira**,[1]

[1]CICS-UBI – Health Sciences Research Centre, Universidade da Beira Interior, Av. Infante D. Henrique, 6200-506 Covilhã, Portugal

[2]CIEPQPF – Departamento de Engenharia Química, Universidade de Coimbra, Rua Sílvio Lima, 3030-790 Coimbra, Portugal

*Author for correspondence: Tel.: +351 275 329 002; icorreia@ubi.pt

**Author for correspondence: Tel.: +351 275 329 002; afmoreira@fcsaude.ubi.pt

Aims: To develop a tumor-targeted chemo-photothermal nanomedicine through the functionalization of acridine orange (AO)-loaded gold-core mesoporous silica shell (AuMSS) nanorods with polyethylenimine (PEI) and hyaluronic acid (HA). **Methods:** Functionalization of the AuMSS nanorods was achieved through the chemical linkage of PEI followed by electrostatic adsorption of HA. **Results:** HA functionalization improved AuMSS' cytocompatibility by decreasing blood hemolysis, and PEI-HA inclusion promoted a controlled and sustained AO release. *In vitro* assays revealed that HA functionalization increased the internalization of nanoparticles by human negroid cervix epithelioid carcinoma cancer (HeLa) cells, and the combinatorial treatment mediated by AuMSS/PEI/HA_AO nanorods presented an enhanced effect, with >95% of cellular death. **Conclusion:** AuMSS/PEI/HA_AO formulations can act as tumor-targeted chemo-photothermal nanomedicines for the combinatorial therapy of cervical cancer.

Graphical abstract:

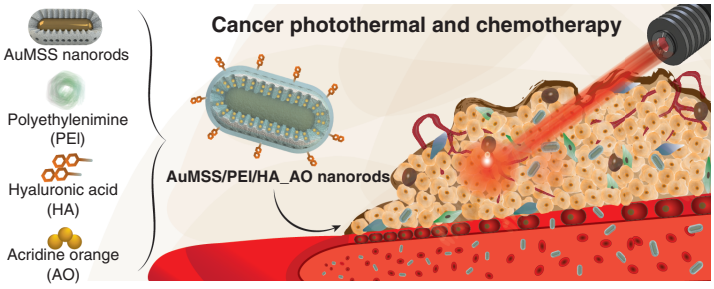

First draft submitted: 23 July 2021; Accepted for publication: 21 October 2021; Published online: 2 December 2021

Keywords: acridine orange • cancer • gold-core silica shell nanoparticles • hyaluronic acid • photothermal therapy • polyethylenimine

Combinatorial therapies mediated by nanomaterials are considered promising approaches for cancer treatment due to potentially fewer side effects, reduced therapeutic dose, bypassing of various cancer cell resistance mechanisms and ultimately enhancing the antitumoral effect [1–3]. One of the most explored combinatorial therapeutic approaches involves the conjugation of chemotherapy with hyperthermia [4,5]. Hyperthermia explores the application of high temperatures, greater than 42°C, that induce cellular damage or even cell death [6,7]. In this field, nanomaterials, due to their capacity to passively accumulate in tumor tissue, can be explored to create a localized temperature increase by generating heat in response to specific stimuli (e.g., near-infrared [NIR] radiation). Thus, this therapeutic modality can specifically induce selective hyperthermia in the cancer tissue while avoiding damage to healthy

tissues [8–10]. Moreover, the combination of photothermal therapy (PTT) with chemotherapeutic agents could induce a synergic therapeutic outcome [11–13]. Carbon nanotubes, graphene oxide and gold are some of the most explored NIR light-responsive nanomaterials that have been developed and applied as photothermal agents [13–16]. Among them, the unique physical and chemical properties of gold-core mesoporous silica shell (AuMSS) nanorods offer high potential for applications in cancer imaging and therapy [14,17]. The rod-shaped gold core possesses an intrinsic capacity to absorb NIR light due to its surface plasmon resonance oscillation, which can convert the light energy into heat (i.e., PTT) and consequently mediates cancer cells' sensitization to chemotherapy and even their destruction [14,18,19]. Furthermore, the AuMSS tubular pores allow the encapsulation of therapeutic molecules while simultaneously increasing the photostability of the gold core [17,20,21]. Nevertheless, despite several studies showing the potential of these nanomedicines to deliver therapeutics and kill cancer cells both *in vitro* and *in vivo*, the application of AuMSS nanorods is hindered by the suboptimal pharmacokinetics and lack of control over drug release [21,22].

These limitations can be addressed by the functionalization of the AuMSS nanorods' surface with bioactive polymers [21,22]. These materials can enhance the nanomaterials' colloidal stability, create a barrier that controls the drug release and facilitate the lysosomal escape [23,24]. Furthermore, the introduction of targeting moieties allows the exploration of antigen–antibody or ligand–receptor recognition interactions, which will improve nanomaterials' specificity toward cancer cells [10,21,25].

Therefore, in this work branched polyethylenimine (PEI) and hyaluronic acid (HA) were combined, for the first time, to functionalize AuMSS nanorods and create a tumor-targeted chemo-photothermal nanomedicine. The AuMSS nanorods were loaded with a drug model, acridine orange (AO), an alkaline dye with specific accumulation in acidic environments, similar to those found at tumor tissue [26,27]. Moreover, AO can interact with DNA through electrostatic interaction or intercalation with the double-helix DNA structure, which can result in cell death [28,29]. Otherwise, PEI is a cationic polymer widely used in gene delivery [24,30]. In this work, PEI was linked to the surface of mesoporous silica, which creates a polymeric barrier, blocking the nanomaterial's pores and controlling the AO release. Additionally, PEI's amine groups are easily protonated in acidic environments, which can enhance the nanomaterials' escape from endocytic vesicles and/or lysosomes (i.e., proton sponge effect) [31]. In addition, HA is a biocompatible and biodegradable polysaccharide that is recognized by the CD44 receptor (overexpressed in the membrane of different cancer cells), rendering a targeting ability to the AuMSS nanorods [13,25,32,33]. The functionalization of the AuMSS nanorods' surface was achieved through chemical linkage of a PEI–silane derivative, followed by electrostatic adsorption of HA. The PEI–HA functionalization did not affect the photothermal potential of AuMSS nanorods and further improved the AO loading capacity. Moreover, the stability of the AuMSS nanorods' PEI–HA functionalization was demonstrated at both pH 7.4 and 5.6 for 28 h, which translated to a sustained AO release over 48 h. Additionally, the studies performed in human negroid cervix epithelioid carcinoma (HeLa) cells revealed that the HA functionalization increased the internalization and specificity of nanomaterials, whereas the chemo-photothermal combinatorial therapy enhanced the therapeutic efficacy of the AuMSS-based nanomaterials (HeLa cells viability ~5%).

Materials & methods

Materials

AO (purity >98%) and HA (Mw 8000–15,000 g/mol) were obtained from Carbosynth (Berkshire, UK). Hydrogen tetrachloroaurate (III) hydrate (99.9% metal basis and Au 49%) were obtained from Alfa Aesar (Kandel, Germany). Hexadecyltrimethylammonium bromide (CTAB, purity 98%) was purchased from Tokyo Chemical Industry (Tokyo, Japan). Tetrahydrofuran (THF) and tetraethylorthosilicate (TEOS, purity >97%) were acquired from Acros Organics (Geel, Belgium). Methanol and hydrochloric acid (HCl) were obtained from VWR International (Carnaxide, Portugal) and Panreac (Barcelona, Spain), respectively. L-ascorbic acid, branched PEI (Mw ~1250 g/mol), 3-(triethoxysilyl)propyl isocyanate (TESPIC, purity 95%), sodium borohydride ($NaBH_4$), silver nitrate ($AgNO_3$), ethanol (EtOH), fluorescein 5-isothiocyanate (FITC), paraformaldehyde (PFA), resazurin, trypsin, Dulbecco's modified eagle medium/nutrient mixture F-12 (DMEM-F12), DMEM-high glucose (DMEM-HG) were obtained from Sigma-Aldrich (Sintra, Portugal). Fetal bovine serum (FBS) was bought to Biochrom AG (Berlin, Germany), and cell imaging plates were acquired from Ibidi GmbH (Munich, Germany). Cell culture t-flasks, propidium iodide (PI), Calcein-AM, Hoechst 33342® and wheat germ agglutinin conjugate Alexa 594® (WGA-Alexa Fluor® 594) were purchased from Thermo Fisher Scientific (Porto, Portugal). HeLa cells

(ATCCs CCL-2) were acquired from ATCC (Middlesex, UK), and primary normal human dermal fibroblast (FibH) cells were purchased from Promocell (Heidelberg, Germany).

Synthesis of AuMSS nanorods

The rod-shaped AuMSS nanoparticles were obtained in a two-step methodology as previously described [12,24,34]. For this purpose, small gold spheres (seeds) were obtained by adding $NaBH_4$ (0.01 M) to a solution containing $HAuCl_4$ (0.0005 M) and CTAB (0.20 M). After 6 h at 30°C, the seed solution was added to a growth solution, which contained 0.03 ml of $AgNO_3$ (0.1 M), 0.21 ml of L-ascorbic acid (0.08 M), 0.3 ml $HAuCl_4$ (0.05 M) and 200 ml of CTAB (0.2 M) and reacted overnight.

The gold nanorods were recovered by centrifugation (12,000×*g*, 20 min at 25°C) removing the excess of CTAB and resuspended in ultrapure water. Subsequently, CTAB (0.01 M) and NaOH (0.1 M) were added to the gold nanorods and stirred for 30 min at 40°C. Three injections of TEOS (0.03 ml, 20% v/v in methanol) were performed in 30-min intervals to create the mesoporous silica shell.

The AuMSS nanorods were recovered by centrifugation (12,000×*g* for 20 min at 25°C), and the cytotoxic CTAB surfactant was removed by adapting a solvent-based approach, as described by Moreira *et al.* [35]. Briefly, several washing cycles based on the AuMSS nanorods' incubation and sonication with a HCl solution (7.5% v/v in EtOH) were performed. The final AuMSS nanorods were recovered by centrifugation (18,000×*g*, 20 min at 25°C) after two additional washing steps with EtOH (99.9% v/v) and two more with ultrapure water.

Synthesis of silane-modified PEI

Branched PEI was chemically modified with TESPIC to enable its posterior grafting on the surface of the AuMSS nanorods [24] (Supplementary Figure 1). Briefly, PEI (0.1 ml) was dissolved in 30 ml of dried THF under magnetic stirring and nitrogen atmosphere at room temperature for 6 h. TESPIC (0.05 ml) was then added to the PEI solution and left to react for 24 h. Afterward, the solvent was evaporated (Rotavap®R-215, Büchi, Switzerland), and the silane-modified PEI (PEI-TESPIC) was resuspended in ultrapure water, dialysed and freeze-dried. The PEI modification with TESPIC was confirmed by Fourier transform infrared spectroscopy (FTIR; Supplementary Figure 2).

Preparation of PEI & HA functionalized AuMSS nanorods

AuMSS nanorods (20 mg) were resuspended in EtOH (33% v/v in ultrapure water, pH 4) and sonicated for 10 min [12,24]. Subsequently, 10 mg of PEI-TESPIC polymer were added to the nanoparticles' solution and left under magnetic stirring. After 24 h, the functionalized AuMSS/PEI nanoparticles were recovered by centrifugation (6000×*g*, for 20 min at 25°C) and washed several times with ultrapure water to remove the unlinked PEI-TESPIC chains. The HA was then immobilized on the surface of AuMSS/PEI nanoparticles by exploring electrostatic interactions between the positively charged amine groups on PEI and negatively charged hydroxyl groups on HA (Supplementary Figure 3). For that purpose, AuMSS/PEI nanoparticles were resuspended in an HA solution (ratio 3:1 w/w), vortexed for 1 min and centrifuged (6000×*g* for 20 min at 25°C). The obtained AuMSS/PEI/HA nanomaterials were washed with ultrapure water to remove the excess of HA.

Characterization of nanoparticles' physicochemical properties

The size and morphology of AuMSS and AuMSS/PEI/HA nanomaterials were evaluated by transmission electron microscopy (TEM; TECNAI G2 20 S-TWIN, EI Company, Amsterdam, The Netherlands). Briefly, a small drop of the nanoparticles' solution was placed in formvar-coated copper grids and dried at room temperature. TEM images were then acquired at an accelerating voltage of 200 kV. The nanomaterials' overall size, gold core size and silica shell thickness were measured using the Image J software (Image J 2.0.0 NIH Image, MD, USA; n = 200). The confirmation of the successful preparation of AuMSS/PEI/HA nanomaterials was performed via FTIR. The FTIR spectra of the different AuMSS-based nanomaterials was acquired on a Nicolet iS10 spectrometer, with a 4 cm^{-1} spectral resolution from 600 to 4000 nm (Thermo Fisher Scientific Inc. MA, USA), and the data were analyzed in the OMNIC spectra software (Thermo Fisher Scientific). The AuMSS, AuMSS/PEI and AuMSS/PEI/HA nanomaterials' surface charge was measured using a Zetasizer Nano ZS equipment (Malvern Instruments, Worcestershire, UK). Additionally, preliminary stability studies of the nanomaterials' surface functionalization were performed by monitoring the changes on the zeta potential upon dispersion in phosphate-buffered saline (PBS; pH 5.6 or 7.4) for 28 h. Thermogravimetric analysis (TGA) was also performed to determine the polymeric content on

AuMSS/PEI/HA nanomaterials. For that purpose, the samples were heated up to 600°C at a rate of 10°C/min using an SDT Q600 equipment (TA Instruments, DE, USA), under inert atmosphere, and weight loss was monitored. Finally, the NIR absorption capacity of the nanomaterials was evaluated through the acquisition of the nanomaterials' UV-Vis-NIR spectrum (Thermo Scientific Evolution 201, Thermo Fisher Scientific Inc.).

Preparation of AO-loaded AuMSS-based nanomaterials

AO-loaded AuMSS-based nanomaterials were obtained through an impregnation methodology as described elsewhere [24,27]. Briefly, AuMSS-based nanomaterials were resuspended in an AO solution (40 μg/ml in methanol), sonicated for 15 min and stirred for 48 h at room temperature. The AO-loaded AuMSS-based nanomaterials (AuMSS_AO and AuMSS/PEI/HA_AO) were then recovered by centrifugation (18,000×*g*, 20 min at 4°C) and freeze-dried. The supernatant was stored and used to quantify the amount of AO encapsulated in the nanomaterials, measuring the supernatant absorbance at 489 nm (Thermo Scientific Evolution 201 Bio UV-vis Spectrophotometer) and a calibration curve (ABS = 0.1981[AO] – 0.0033; R^2 = 0.999). The encapsulation efficiency (%EE) of AO was then calculated through the following equation [27]:

$$\%EE = \frac{(\text{Initial AO weight} - \text{AO weight in the supernatant})}{\text{Initial AO weight}} \times 100 \qquad \text{(Equation 1)}$$

In vitro drug release

AO-loaded AuMSS-based nanomaterials were resuspended in PBS and inserted in a Float-A-Lyzer dialysis bag [12]. The dialysis was performed in PBS at pH 5.6 or 7.4 under magnetic stirring at 37°C. At different time points, 1 ml of the dialysate was collected and replaced with fresh PBS. Subsequently, the released AO was determined by the UV-Vis methodology described earlier.

In vitro photothermal capacity of AuMSS-based nanomaterials

The AuMSS and AuMSS/PEI/HA nanomaterials photothermal capacity was recorded using a thermocouple sensor with an accuracy of 0.1°C [12,34]. Briefly, the AuMSS-based nanomaterials (200 μg/ml) were irradiated with a NIR laser (808 nm, 1.7 W/cm^2). The temperature variations were recorded at different time points from 1 to 10 min. Ultrapure water exposed to NIR light was used as a control group. Additionally, the photothermal conversion efficiency of AuMSS-based materials formulations (Supplementary Figure 4) was calculated according to the equations described in the supporting information.

Cytocompatibility & hemocompatibility assays

The cytocompatibility of AuMSS-based nanomaterials was evaluated on both FibH and HeLa cells using the resazurin assay [36]. Briefly, FibH or HeLa cells were seeded in 96-well flat-bottom culture plates (10,000 cells/well, 100 μl of DMEM-F12 or DMEM-HG) and incubated for 48 h in a humid atmosphere (37°C, 5% CO_2). Afterward, the medium was replaced, and the cells were incubated with AuMSS and AuMSS/PEI/HA nanomaterials at different concentrations (25–200 μg/ml). Subsequently, at 24, 48 and 72 h of incubation the cell viability was determined by the resazurin assay – that is, incubation of culture medium containing 10% (v/v) of resazurin (1 mg/ml) in the dark at 37°C for 4 h and measurement of the fluorescence at an excitation/emission wavelength of λ = 560 nm and λ = 590 nm (Spectramax Gemini XS microwell plate reader, Molecular Devices LLC, CA, USA). Negative control (K^-) cell only exposed to culture medium; positive control (K^+) cells incubated with EtOH (99.9%).

The hemocompatibility was assessed by determining the blood hemolysis upon incubation with AuMSS-based nanomaterials [12,24]. Briefly, red blood cells (RBCs) obtained from adult mice were incubated at room temperature at different concentrations (50, 100 and 200 μg/ml in PBS) of AuMSS, AuMSS/PEI and AuMSS/PEI/HA nanomaterials for 4 and 24 h. At the predetermined incubation times, the samples were centrifuged (500×*g*, 4°C for 5 min) and 100 μl of the supernatant were transferred to a 96-well plate to measure the hemoglobin absorbance at 570 nm. The percentage of RBC hemolysis was determined through the following equation [12]:

$$\text{Hemolysis}(\%) = \frac{\text{Sample Abs} - \text{Negative Control Abs}}{\text{Positive Control Abs} - \text{Negative Control Abs}} \times 100 \qquad \text{(Equation 2)}$$

Evaluation of nanoparticles' cellular uptake

The uptake of AuMSS-based nanomaterials by HeLa or FibH cells was assessed by fluorescence spectroscopy and confocal microscopy [12]. FibH or HeLa cells were seeded into 96-well flat-bottom culture plates (10,000 cells/well,

100 µl of DMEM-F12 or DMEM-HG) and incubated for 48 h in a humid atmosphere (37°C, 5% CO_2). Then, the culture media was replaced and FITC-stained AuMSS or AuMSS/PEI/HA nanomaterials at a concentration of 200 µg/ml were incubated for 4 h. Additionally, in one of the test groups, the cells were pretreated with HA (200 µg/ml), 4 h before the incubation with AuMSS-based nanomaterials. Afterward, cells were washed with ice-cold Krebs ringer buffer (KRB) to remove the non-internalized nanoparticles and lysed with Triton X-100 (1% in KRB for 30 min at 37°C). Cells only incubated with KRB were used as a negative control. The FITC fluorescence (λ_{ex} = 490 nm and λ_{em} = 520 nm) was then quantified using a spectrofluorometer (Spectramax Gemini XS, Molecular Devices LLC, CA, USA).

In the confocal laser scanning microscopy (CLSM) experiments, HeLa cells were seeded on µ-Slide 8-well Ibidi imaging plates (15,000 cells/well, 200 µl of DMEM-HG) and incubated at 37°C for 48 h [37]. The medium was then removed and FITC-stained AuMSS-based nanomaterials (200 µg/ml) were incubated for 4 h. Cells were washed with PBS, fixed with PFA (4% w/v) for 10 min and washed again with PBS. Subsequently, cells were treated with WGA-Alexa Flour® 594 and Hoechst 33342® for the cytoplasm and nucleus staining, respectively. The CLSM images were obtained using a Zeiss LSM 710 confocal microscope (Carl Zeiss SMT Inc., Jena, Germany) and the image analysis was performed in the Zeiss Zen 2010 software.

Evaluation of 2D therapeutic effect of the AuMSS nanoparticles

2D characterization of the AuMSS in vitro cytotoxic activity

The cytotoxic effect of AO-loaded AuMSS-based nanomaterials was evaluated on HeLa cells through the resazurin assay [12]. Briefly, HeLa cells were seeded in 96-well flat-bottom culture plates (10,000 cells/well, 100 µl of DMEM-HG) and incubated for 48 h. Different concentrations (100 and 200 µg/ml with or without AO) of AuMSS-based nanomaterials were incubated for 4 h. After this, the cells were irradiated with a NIR laser (808 nm, 1.7 W/cm^2) for 5 min. At 48 h of incubation, the cell viability was determined by using the resazurin assay as described earlier. Cells not incubated with nanomaterials and irradiated were used as control (K^- NIR), whereas cells incubated with EtOH (99.9%), and cells cultured only with culture medium were used as positive (K^+) and negative (K^-) controls, respectively.

Additionally, the IC_{50} of AO in HeLa cells was also determined via resazurin assay. Briefly, the HeLa cells viability was assessed after incubation with increasing AO concentrations (0.1–200 µM) for 48 h. Then, the obtained results were used to plot the AO's dose–response curve in the OriginLab software (Supplementary Figure 5).

Live/dead assay

The photothermal effect of the AuMSS-based nanomaterials was further characterized through the live/dead assay (Invitrogen/Life Technologies, CA, USA) [25]. For this purpose, HeLa cells were seeded on µ-Slide 8-well Ibidi imaging plates (15,000 cells/well, 200 µl of DMEM-HG) and incubated at 37°C in a humidified atmosphere (5% CO_2). After 48 h, the cells were incubated with AuMSS-based nanomaterials at 200 µg/ml for 4 h, followed by irradiation with a NIR laser (808 nm, 1.7 W/cm^2) for 5 min. Afterward, cells were stained with Calcein AM and PI to allow the visualization of live and dead cells, respectively. Finally, the live/dead images were obtained by CLSM (Zeiss LSM 710).

Statistical analysis

Data are presented as the mean ± standard deviation (SD). The statistical analysis of experiments with two groups was performed with the unpaired Student t-test. One-way analysis of variance (ANOVA) with the Student–Newman–Keuls post-test was used for multiple group comparison. A p-value lower than 0.05 was considered statistically significant. Statistical analysis was performed using GraphPad Prism v.7.0 software (Trial version, GraphPad Software, CA, USA).

Results

Synthesis & characterization of AuMSS-based nanomaterials

The TEM images clearly show the core-shell organization of the AuMSS nanomaterials, presenting a denser core, a single gold nanorod, coated with a uniform mesoporous silica shell (Figure 1A). Moreover, the size measurements performed in the ImageJ software (Figure 1B) show that the rod-like gold core presents a length and width of 51 ± 5 and 17 ± 2 nm, respectively. The mesoporous silica shell presented a mean thickness of 24 ± 5 nm, resulting in an

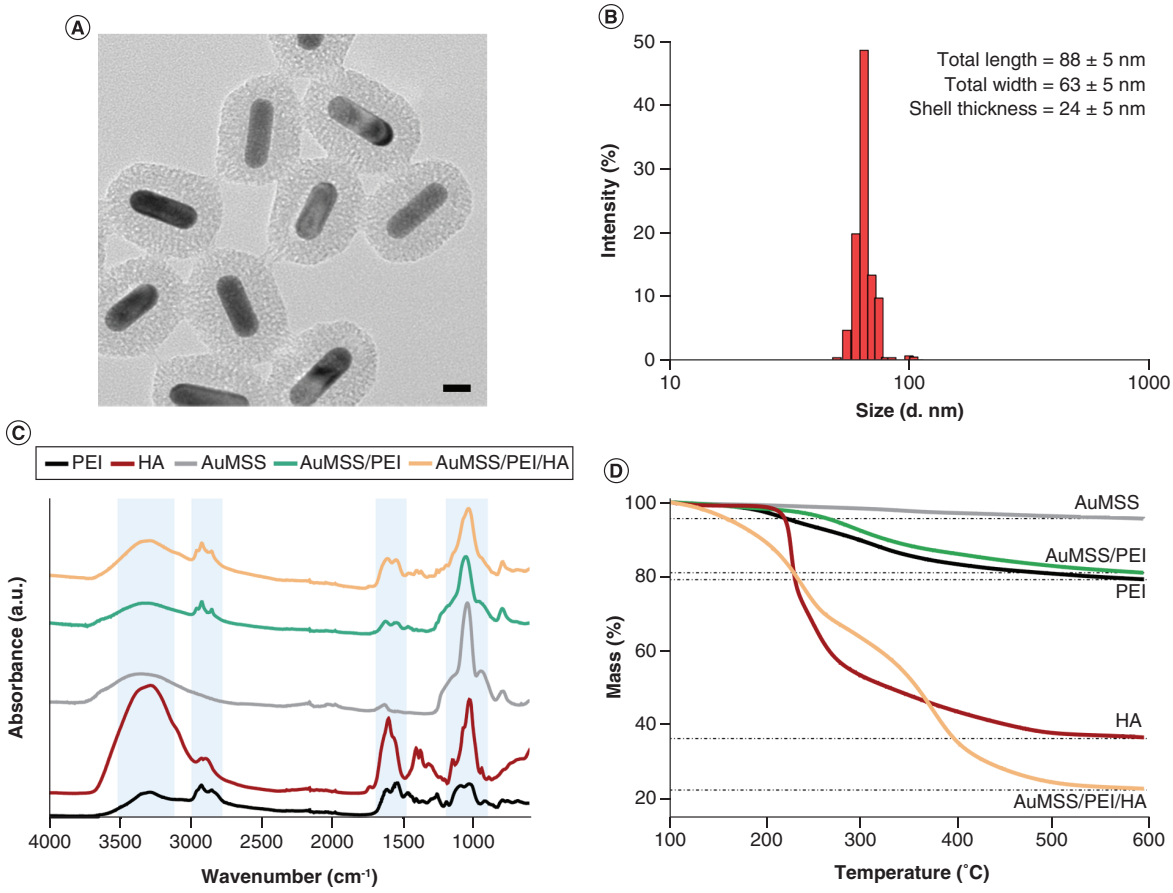

Figure 1. Physicochemical characterization of gold-core mesoporous silica shell-based nanomaterials. (A) Transmission electron microscopy image of AuMSS nanorods. Scale bar corresponds to 20 nm. **(B)** AuMSS nanorods' size distribution (length and width included), n = 200. **(C)** Fourier transform infrared spectra of AuMSS-based nanomaterials, PEI and HA polymers. **(D)** Thermogravimetric analysis of AuMSS-based materials, PEI and HA polymers. AuMSS: Gold-core mesoporous silica shell; HA: Hyaluronic acid; PEI: Polyethylenimine.

overall particle size of the AuMSS nanorods of 88 ± 5 nm in length and 63 ± 5 nm in width. The TEM images and size measurements also confirm the homogeneity in both size and structure of nanomaterials.

The FTIR spectrum of AuMSS nanorods showed the characteristic Si-O, Si-OH and Si-O-Si vibrations at the 1100–750 cm^{-1} region (Figure 1C). The absence of the CTAB characteristic bands at 1450–1500 cm^{-1} (CH_3-N^+ deformation) and 2850–2950 cm^{-1} (C-H vibration) further indicates the success of the purification step [34]. The postsynthesis grafting of the silane-modified PEI in AuMSS nanorods was confirmed by the presence of C-H stretching vibrations around the 3000–2885 cm^{-1} region as well as N-H deformation vibration in the 1700–1400 cm^{-1}. Additionally, an increase in the ratio between the Si-O-Si and Si-OH peaks was also detected at 1045 cm^{-1} and 950 cm^{-1}, respectively, an indicator of the TESPIC-PEI condensation at the surface of the mesoporous silica shell [24]. In turn, the HA introduction via electrostatic interactions with positively charged PEI amine groups resulted in the presence of HA's CO-NH (amide) and OH characteristic peaks around the 1630–1680 cm^{-1} and 3600–3000 cm^{-1} regions [38].

The surface charge' measurements were also performed to monitor the functionalization of AuMSS nanorods (Figure 2B). The AuMSS nanorods present a negative surface charge of -28 ± 2 mV, and the subsequent modification with PEI increased the nanomaterials surface charge to 44 ± 3 mV. This charge was reversed upon electrostatic binding of HA to the AuMSS/PEI nanoparticles, with the neutralization of the surface charge to -10 ± 2 mV. Simultaneously, the stability of the PEI-HA functionalization was also evaluated by studying the changes on the nanomaterials' surface charge upon incubation at two pH values, 7.4 (physiological conditions) and 5.6 (tumor microenvironment) for 24 h, followed by 2 h at pH 7.4 and 2 h at pH 5.6 (Figure 2C & D). The obtained results

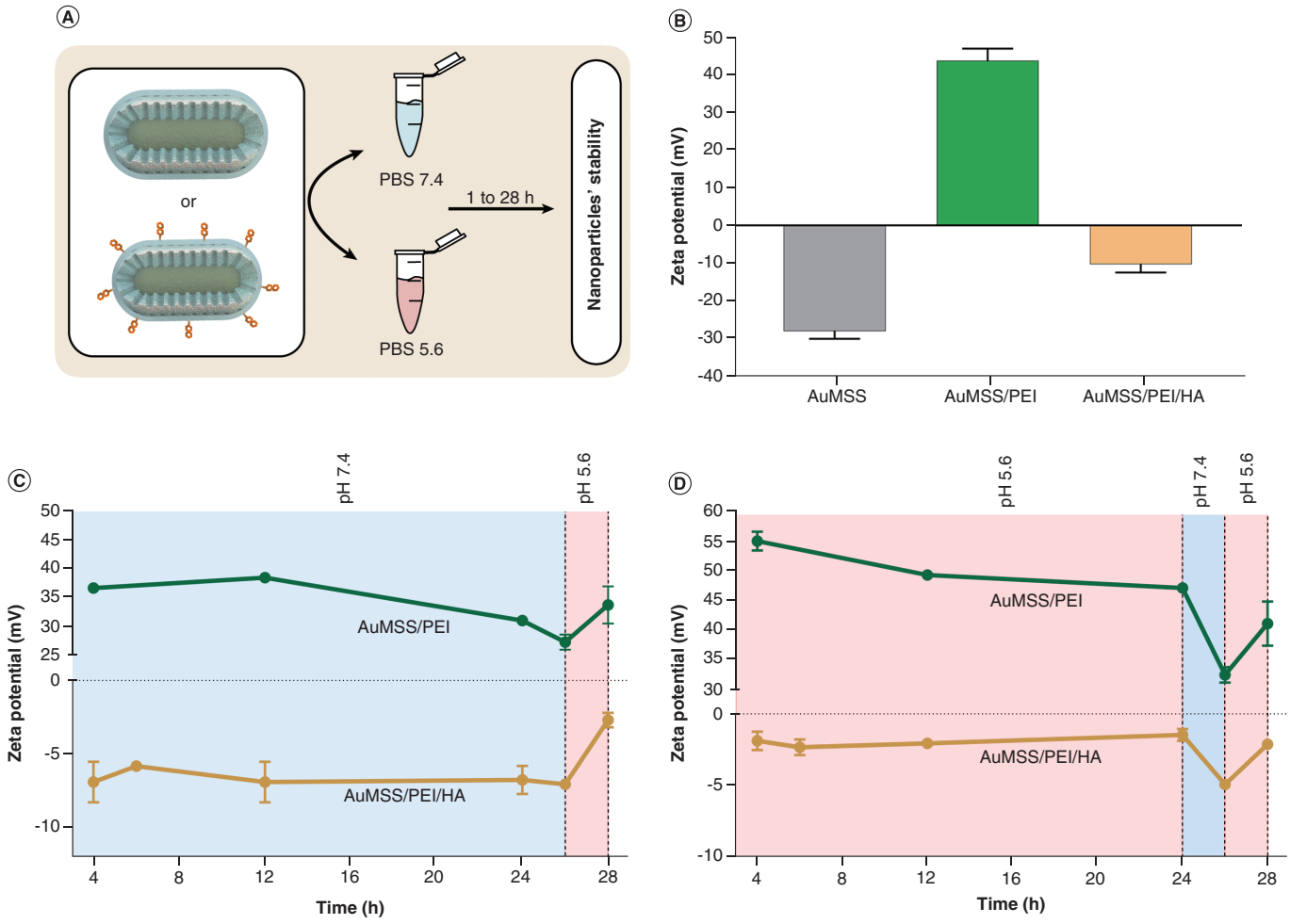

Figure 2. Characterization of nanoparticles surface charge and stability. (A) Schematics of the nanoparticles' stability methodology. **(B)** Surface charge analysis of AuMSS, AuMSS/PEI and AuMSS/PEI/HA nanorods. **(C)** Surface charge variation (analysis of stability) of AuMSS/PEI and AuMSS/PEI/HA nanorods when dispersed in PBS at pH 7.4 **(C)** or 5.6 **(D)**. Data are presented as mean ± standard deviation, n = 3.
AuMSS: Gold-core mesoporous silica shell; HA: Hyaluronic acid; PBS: Phosphate-buffered saline; PEI: Polyethylenimine.

show that the incubation of AuMSS/PEI nanomaterials in acidic pH promotes the increase of the surface charge to values ~48–60 mV upon incubation for 26 h, whereas those incubated at pH 7.4 maintained a surface charge ~27–43 mV. Additionally, upon acidification of the media (pH reduced to 5.6 from 26 to 28 h of incubation) occurs an increase of the AuMSS/PEI surface charge from 27 to 35 mV (Figure 2C). Moreover, the AuMSS/PEI/HA nanomaterials maintained the surface charge during the initial 26 h of incubation, -10 mV to -6 mV at pH 7.4, which increased to -2 mV after the media acidification (pH reduced to 5.6 from 26 h to 28 h of incubation). Similar data were observed in the AuMSS/PEI/HA nanomaterials incubated initially at pH 5.6 for 24 h, surface charge -2 mV to -1 mV; this value decreased to -6 mV with incubation at pH 7.4 for 2 h and was reverted to -2 mV with the pH change to 5.6.

Finally, the amount of polymer (PEI and HA) grafted to the AuMSS nanorods was quantified through TGA analysis (Figure 1D). The obtained TGA weight loss curves show that the AuMSS nanorods present a 5% weight loss, whereas the AuMSS/PEI and AuMSS/PEI/HA presented greater weight loss, which represent a polymeric content of 19 and 77%, respectively. The TGA curve profiles of PEI and AuMSS/PEI nanoparticles are similar, however, the TGA curve of AuMSS/PEI/HA nanoparticles present one additional inflection when compared with AuMSS/PEI nanoparticles, which is coincident with the HA degradation.

10.2217/nnm-2021-0270

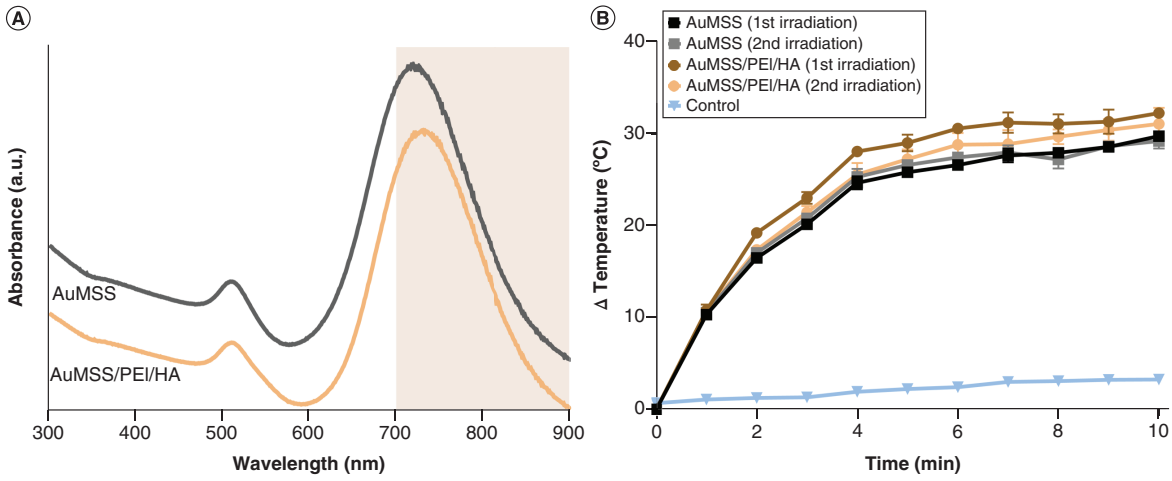

Figure 3. Analysis of gold-core mesoporous silica shell-based nanomaterials' photothermal potential. (A) UV-vis spectra of AuMSS and AuMSS/PEI/HA nanorods. **(B)** Temperature variation curves of the AuMSS formulations resuspended in ultrapure water upon near-infrared radiation laser (808 nm, 1.7 W/cm^2, 10 min) with two irradiation cycles.
AuMSS: Gold-core mesoporous silica shell; HA: Hyaluronic acid; PEI: Polyethylenimine.

Evaluation of the photothermal properties of AuMSS-based nanomaterials

The photothermal potential of the AuMSS-based nanomaterials was initially evaluated through UV-vis-NIR spectroscopy (Figure 3A). The obtained spectra show that both AuMSS and AuMSS/PEI/HA nanomaterials presented the two characteristic peaks of gold nanorods – namely, at 520 nm (transverse plasmon resonance) and 750 nm (longitudinal plasmon resonance). Therefore, the photothermal performance of AuMSS and AuMSS/PEI/HA nanomaterials was evaluated by recording the temperature changes in response to the irradiation with a NIR laser (Figure 3B). Under laser irradiation for 10 min, both formulations promoted an increase in the temperature by ~30°C. Moreover, no significant changes were observed in the heating capacity of AuMSS-based nanomaterials after a second irradiation cycle. The correspondent photothermal conversion efficiency for the AuMSS and AuMSS/PEI/HA nanorods was 65 ± 3 and 71 ± 1%, respectively (Supplementary Figure 4).

AO-loading capacity and release profile of AuMSS nanoparticles

The loading of the AO drug model was achieved via an impregnation method, resulting in encapsulation efficiencies of 56 and 70% for AuMSS and AuMSS/PEI/HA, respectively (Figure 4A). These values correspond to the encapsulation of 18 and 21 μg of AO per mg of AuMSS and AuMSS/PEI/HA, respectively. Subsequently, the release profile of AO from AuMSS-based nanomaterials was characterized at different pH values, 5.6 and 7.4. Figure 4B shows that bare AuMSS nanorods released approximately 80% of the AO content when incubated in both pHs for 48 h. In turn, the PEI-HA functionalization led to a slower and sustained AO release, with 49 and 42% of AO release at pH 5.6 and 7.4, respectively.

Characterization of nanoparticles' biocompatibility

Nanoparticles' cytocompatibility

Before evaluation of the AuMSS-based nanomaterials' cytotoxic capacity, a cytocompatibility study was performed on HeLa and FibH cells. Both cell lines were incubated for 24, 48 and 72 h with different concentrations of AuMSS-based nanomaterials (25–200 μg/ml), and the cell viability was quantified using the resazurin assay. As observed in Figure 5, no significant signs of toxicity were observed in both cell lines, with all the test groups presenting cell viabilities close to 100% during the 72 h of the study.

Hemocompatibility

The safety of AuMSS-based nanomaterials was further characterized in the hemolysis assays (Figure 6A). For that purpose, UV-vis spectroscopy was used to measure the RBC lysis (i.e., hemoglobin release) at 4 and 24 h of incubation with different concentrations (50, 100 and 200 μg/ml) of AuMSS-based nanomaterials (Figure 6B

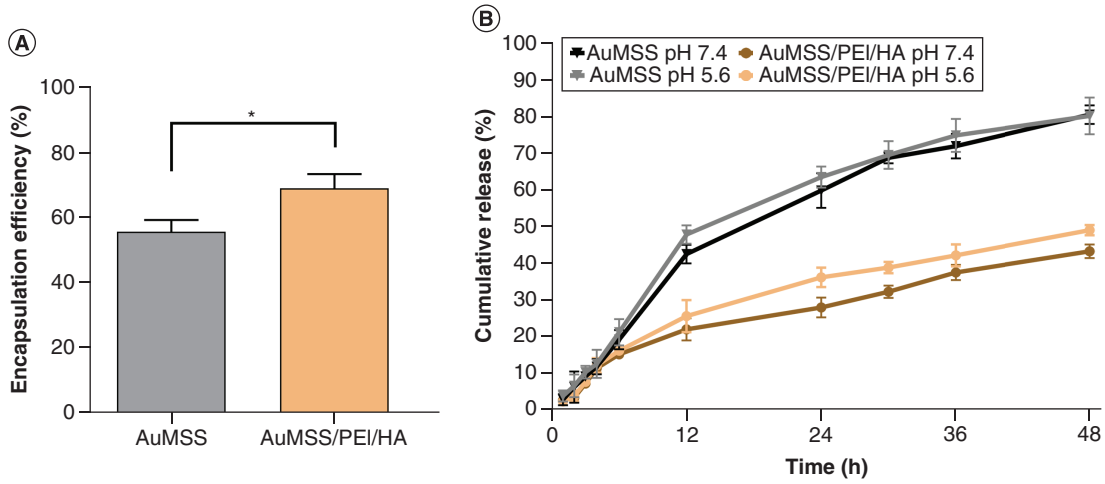

Figure 4. Characterization of acridine orange encapsulation efficiency and release profile. (A) AO encapsulation efficiency in AuMSS and AuMSS/PEI/HA nanoparticles. (B) Analysis of the AO release profile at different pH values (5.6 and 7.4). Data are presented as mean ± standard deviation, n = 3. The Student's t-test was used to compare the results obtained in panel A.
*$p < 0.05$.
AO: Acridine orange; AuMSS: Gold-core mesoporous silica shell; HA: Hyaluronic acid; PEI: Polyethylenimine.

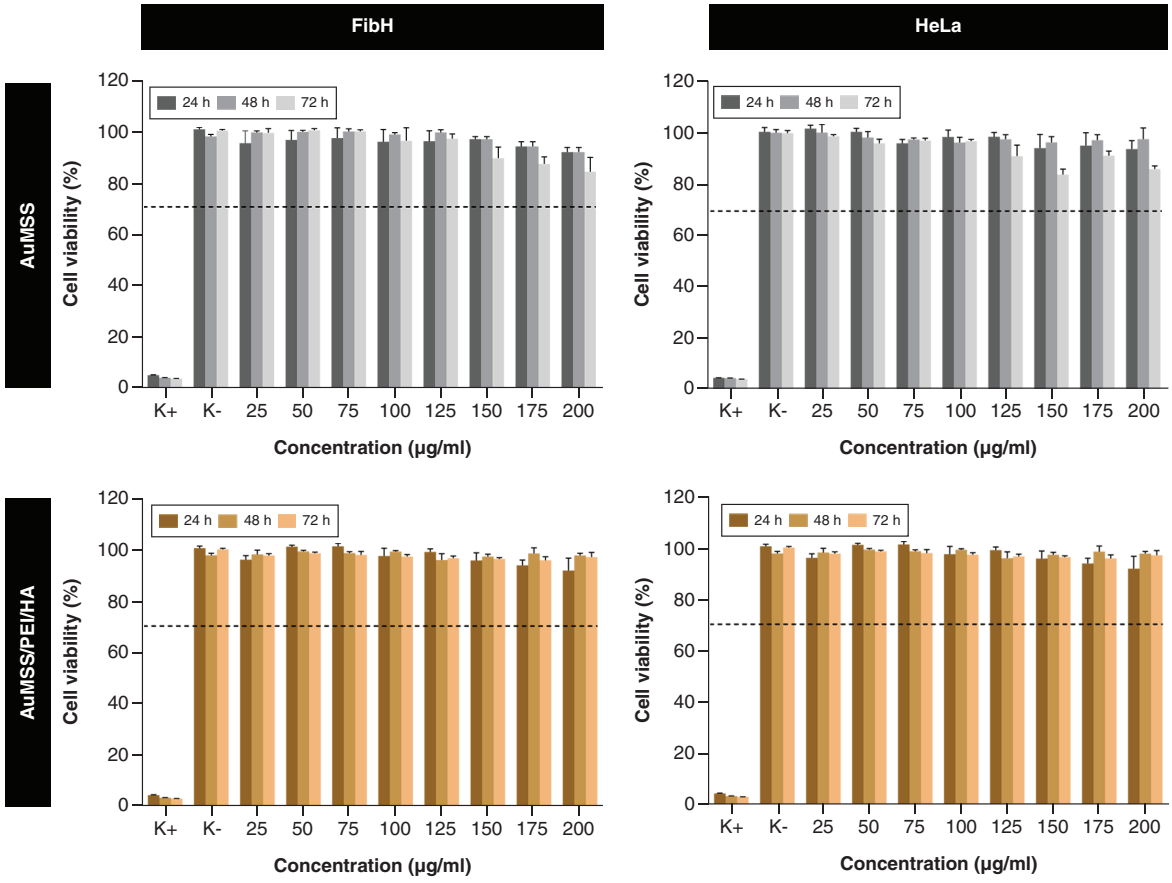

Figure 5. Evaluation of gold-core mesoporous silica shell-based nanomaterials' cytocompatibility in FibH and HeLa cells at 24, 48 and 72 h. Negative control (K-): cells without nanoparticles incubation; positive control (K+): cells treated with ethanol. Data are presented as mean ± standard deviation, n = 5.
AuMSS: Gold-core mesoporous silica shell; HA: Hyaluronic acid; PEI: Polyethylenimine.

10.2217/nnm-2021-0270

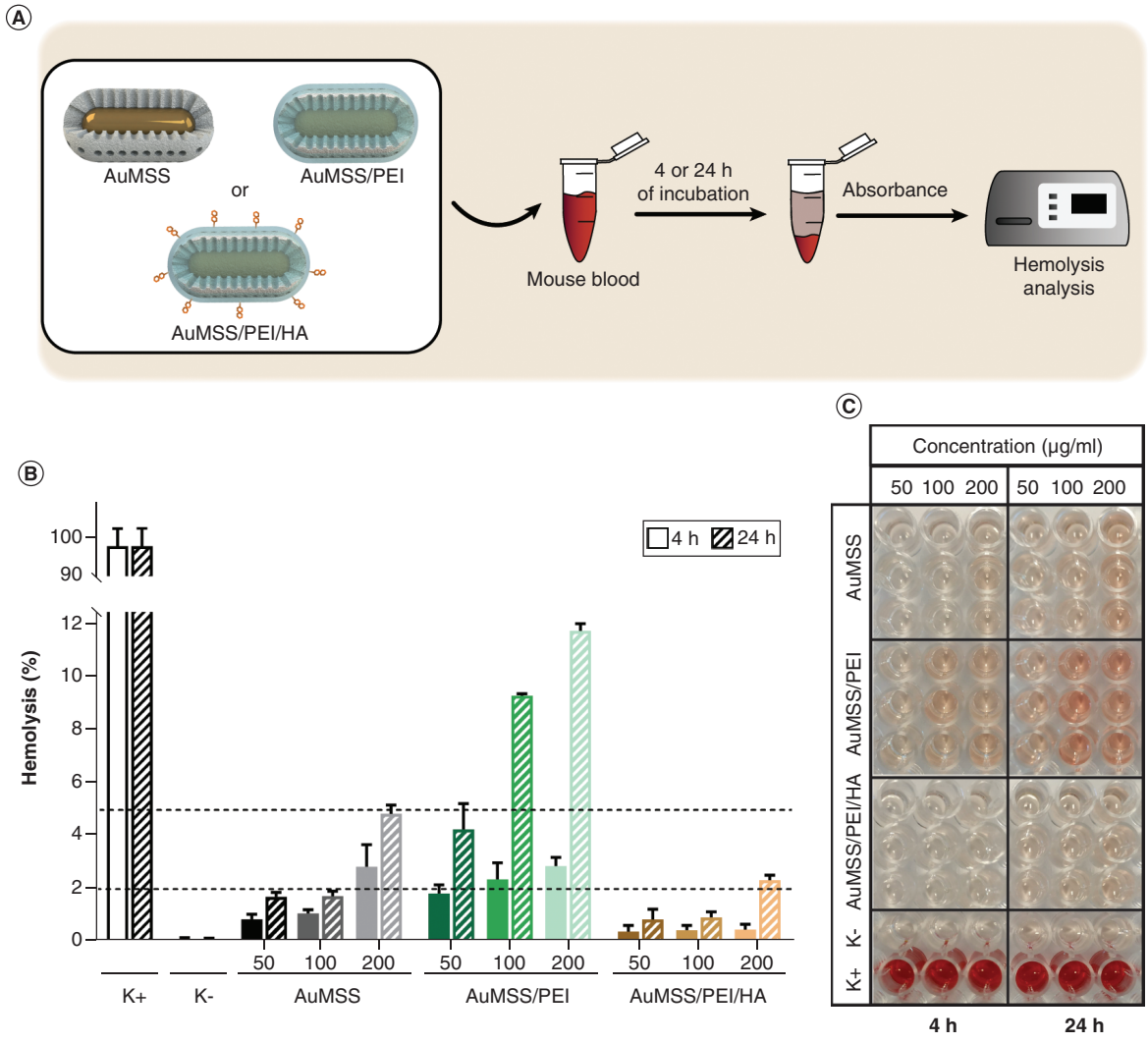

Figure 6. Analysis of the hemocompatibility of gold-core mesoporous silica shell-based nanomaterials. (A) Schematic representation of the methodology. **(B)** Analysis of the red blood cells' lysis upon incubation of AuMSS-based nanomaterials at different concentrations (50, 100 and 200 µg/ml) over 4 and 24 h. **(C)** Optical image of the blood supernatants obtained after the incubation of AuMSS-based nanomaterials. Red blood cells' incubated with Triton-X 100 or phosphate-buffered saline were used as positive (K+) and negative (K-) controls, respectively. Data are presented as mean ± standard deviation, n = 3.
AuMSS: Gold-core mesoporous silica shell; HA: Hyaluronic acid; PEI: Polyethylenimine.

& C & Supplementary Figure 6). The data show a concentration and time-dependent hemolysis, particularly for AuMSS and AuMSS/PEI nanomaterials. The AuMSS nanorods at 200 µg/ml were slightly hemolytic after 4 h of incubation and hemolytic after 24 h of incubation, because more than 5% of hemoglobin was released. Otherwise, the PEI grafting on the surface of the AuMSS nanorods further exacerbated RBC hemolysis at all time points and tested concentrations. However, the HA complexation masked this effect, decreasing the hemolysis values to <0.5% after 4 h of incubation. In the AuMSS/PEI/HA nanomaterials, only a concentration of 200 µg/ml at 24 h of incubation presented a hemolysis value at the borderline of being slightly hemolytic (i.e., 2.3% of hemolysis).

Evaluation of AuMSS nanoformulations' uptake

To evaluate the AuMSS-based nanomaterials' targeting capacity the uptake was evaluated by fluorescence spectroscopy and CLSM (Figure 7A). For that purpose, AuMSS-based nanomaterials were tagged with FITC and incubated with HeLa (CD44 overexpression) or FibH cells (low CD44 expression) by fluorescence spectroscopy (Figure 7B).

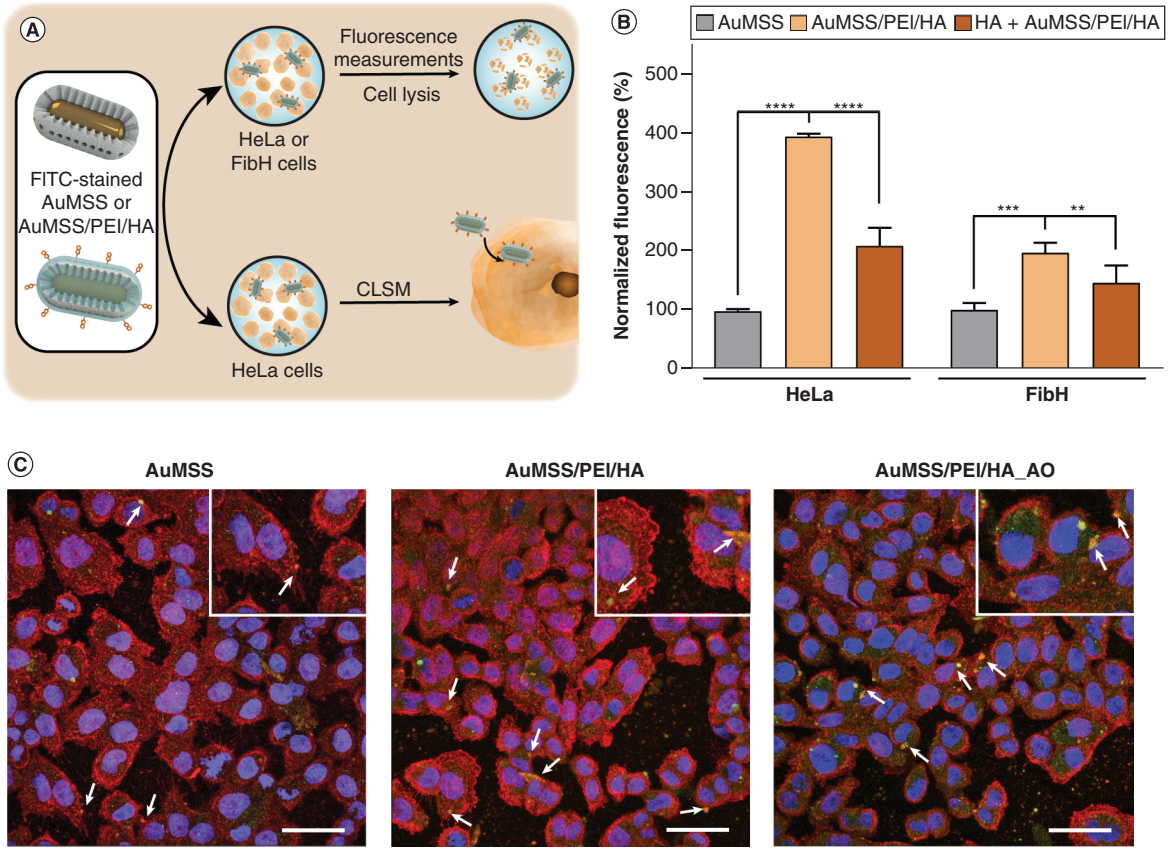

Figure 7. Evaluation of gold-core mesoporous silica shell and AuMSS/PEI/HA nanomaterials' internalization by FibH and HeLa cells. (A) Schematic representation of the uptake experiments. **(B)** Fluorescence spectroscopy analysis of the AuMSS and AuMSS/PEI/HA nanorods' uptake by FibH and HeLa cells. The fluorescence was normalized toward the AuMSS nanorods-treated groups. Data are presented as mean ± standard deviation, n = 5. **(C)** CSLM images of the FITC-stained AuMSS-based nanomaterials' uptake by HeLa cells. The white arrows indicate the internalized nanoparticles. The scale bar = 20 μm. Top right corner: enlarged section of the CLSM image. Red channel: WGA-Alexa Fluor 594®-stained cell cytoplasm; blue channel: Hoechst 33342®-stained cell nucleus; green channel: FITC-stained nanoparticles.
**$p < 0.01$; ***$p < 0.001$; ****$p < 0.0001$.
AO: Acridine orange; AuMSS: Gold-core mesoporous silica shell; CLSM: Confocal laser scanning microscopy; FITC: Fluorescein 5-isothiocyanate; HA: Hyaluronic acid; PEI: Polyethylenimine.

The results demonstrated that the HeLa cells treated with AuMSS/PEI/HA present four-times greater FITC fluorescence than those treated with uncoated AuMSS nanorods. Moreover, the FibH cells also presented an increased uptake of AuMSS/PEI/HA nanoparticles. Nevertheless, the AuMSS/PEI/HA uptake by HeLa cells was two-times greater than that observed in FibH cells. Therefore, to further assess the CD44 influence in the AuMSS-based nanomaterials' uptake, the HeLa and FibH cells were treated with free HA for 4 h before nanomaterials' incubation. This pretreatment with free HA significantly decreased the AuMSS/PEI/HA uptake by HeLa cells (two-times lower), whereas in the FibH group, only a slight reduction of the nanomaterials' uptake was observed. Otherwise, the uptake of the FITC-stained AuMSS-based nanomaterials was also confirmed by CLSM. Figure 7C shows that HeLa cells can successfully uptake all nanomaterials (indicated by the white arrows). Additionally, it is also noticeable that both the AuMSS/PEI/HA and AuMSS/PEI/HA_AO groups present a higher cellular internalization, similar to that observed in the fluorescence spectroscopy data.

Evaluation of 2D therapeutic effect mediated AuMSS nanoformulations

The chemo-photothermal effect of AuMSS-based nanomaterials was evaluated in HeLa cells (Figure 8 & Supplementary Figure 7) after nanomaterials' incubation (100 and 200 μg/ml), with or without NIR-laser irradiation (808 nm, 1.7 W/cm^2, for 5 min). Figure 8B shows that both AO delivery and the photothermal effect alone can

10.2217/nnm-2021-0270

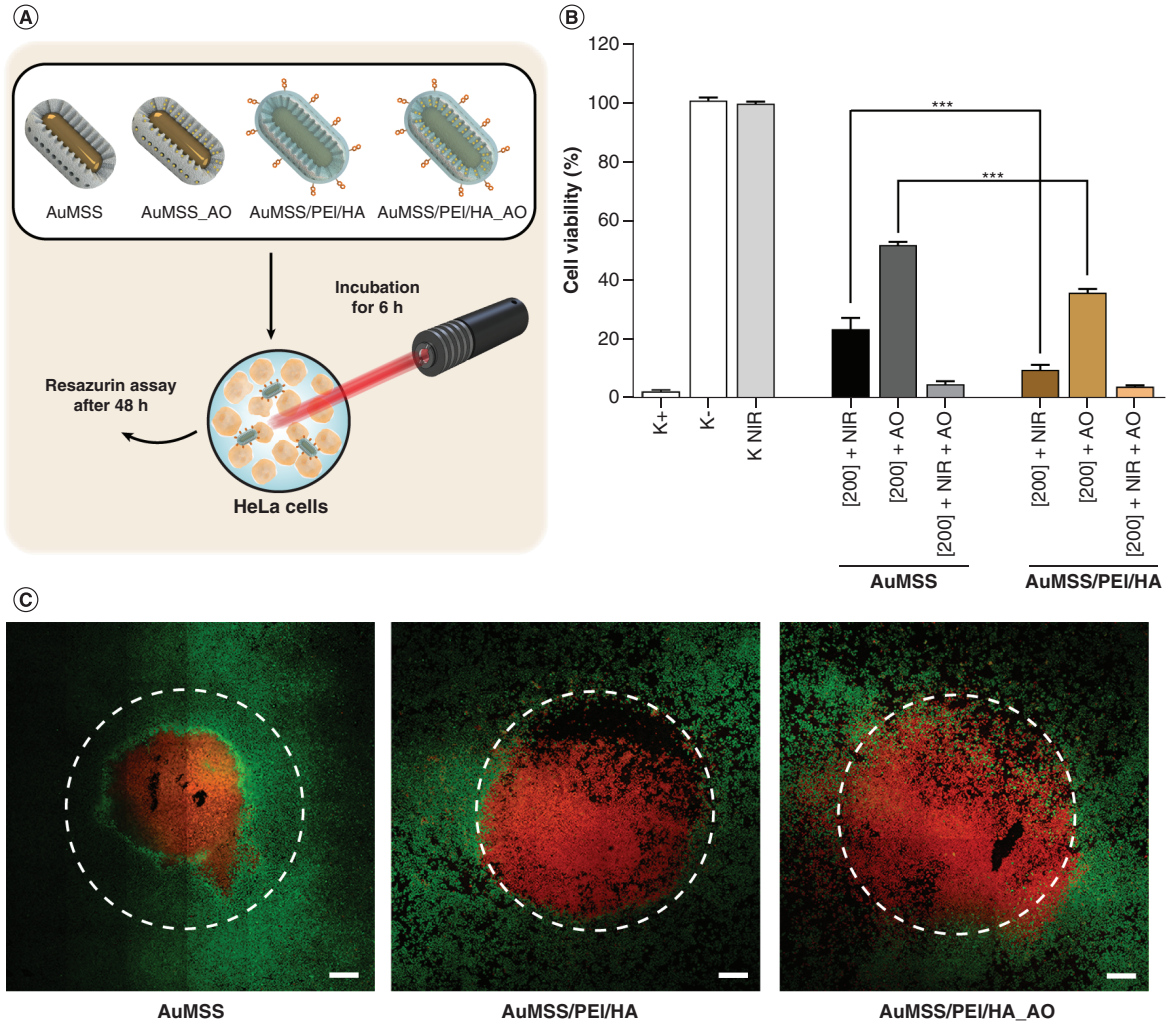

Figure 8. Analysis of the gold-core mesoporous silica shell-based nanomaterials therapeutic potential in HeLa cancer cells. (A) Schematic representation of the AuMSS-based nanomaterials' cytotoxic experiments upon NIR-laser irradiation (808 nm, 1.7 W/cm^2, 5 min). **(B)** Analysis of the cytotoxic activity of AuMSS and AuMSS/PEI/HA (200 μg/ml), with or without AO encapsulation or NIR-laser irradiation (5 min). Negative control (K-): cells without nanoparticles incubation; NIR control (K NIR): cells without nanoparticles incubation and irradiated with NIR laser (808 nm, 1.7 W/cm^2, 5 min). Data are presented as mean ± standard deviation, n = 5. **(C)** Live/dead CLSM images of the cytotoxic activity of AuMSS-based nanomaterials at 200 μg/ml. The white circles represent the total area irradiated by the NIR laser. Red channel: PI-stained cells; green channel: Calcein-AM stained cells. Scale bar = 500 μm. ***$p < 0.001$.
AO: Acridine orange; AuMSS: Gold-core mesoporous silica shell; HA: Hyaluronic acid; NIR: Near-infrared; PEI: Polyethylenimine; PI: Propidium iodide.

decrease the viability of HeLa cells. The HeLa cells treated with the standalone therapies using AuMSS nanorods (200 μg/ml) presented cell viability of 23 and 52% for PTT and AO delivery, respectively. In turn, the standalone therapies mediated by AuMSS/PEI/HA nanomaterials (200 μg/ml) resulted in HeLa cell viabilities of 10 and 35% for single PTT and chemotherapy, respectively. The combination of PTT and AO in both AuMSS and AuMSS/PEI/HA improved the therapeutic effect of the nanoparticles, with >95% of cellular death at 200 μg/ml. Moreover, it is also possible to observe the benefits of the PEI-HA functionalization since the standalone therapies mediated by the AuMSS/PEI/HA nanomaterials presented lower values of viable cells.

Live/dead assays (Figure 8C) also confirmed the immediate cell death in response to the NIR-laser irradiation. The CLSM images show a zone with a high number of dead cells (red fluorescence) in all the AuMSS-based nanomaterials, which is within the area irradiated by the NIR laser (identified with the white circles). Moreover, it is possible to observe that AuMSS/PEI/HA nanomaterials present a higher number of PI-stained HeLa cells,

whereas the AuMSS/PEI/HA_AO-treated group shows a zone with dead cells that exceed the zone irradiated by the NIR laser.

Discussion

The preparation of AuMSS-based nanomaterials started with the production of the gold nucleus with a rod-like shape followed by the coating with a mesoporous silica shell [17,34]. The rod-like gold nucleus was obtained by promoting the growth of small gold spheres (seeds), in the presence of silver nitrate and ascorbic acid. Afterward, the TEOS hydrolysis and condensation at the gold nanorods surface created a mesoporous silica shell, using CTAB micelles as a pore template [21,34]. The cytotoxic CTAB surfactant was removed by adapting a solvent-based approach, and its successful removal was confirmed (absence of their two characteristic bands at 1450–1500 cm^{-1} and 2850–2950 cm^{-1}) in the FTIR spectra of AuMSS-based nanomaterials (Figure 1C) [34]. Additionally, the AuMSS nanorods homogeneity was observed both in size and structure, resulting in an aspect ratio (AR) of approximately 3.1, which is within the range compatible with NIR light absorption and photothermal applications (Figure 1A & B) [39,40]. These data are congruent with previous reports and similar synthesis methodologies described in the literature [25,41]. For example, Jacinto *et al.* reported the production of rod-shaped AuMSS with an AR of 3.1, and a total length and width of 85 ± 12 and 64 ± 8 nm, respectively, using a similar synthesis methodology [25]. Recently, Cheng *et al.* adapted this synthesis process to produce AuMSS nanomaterials with a total length and width of 78 ± 4.2 and 49 ± 3.5 nm, respectively. Additionally, the average width and length of the gold core were 12 ± 1.3 and 39 ± 2.5 nm, respectively, resulting in an AR of ∼3.2 [41]. Moreover, this size range allows the nanomaterials to explore the enhanced permeability and retention effect, and consequently present a passive accumulation in tumor tissue [10,42].

The AuMSS nanorods were then modified with the silane-modified PEI through a postsynthesis grafting methodology followed by electrostatic adsorption of HA. The increase of the nanoparticles' surface charge after PEI modification (from -28 to 44 mV) is congruent with the introduction of the PEI's high number of cationic protonatable amine moieties, which supports the successful grafting of silane-modified PEI on the nanoparticles (Figure 2B). Similarly, the posterior electrostatic binding of HA to AuMSS/PEI nanoparticles was confirmed by the neutralization of nanoparticles' surface charge (-10 ± 2 mV), which is attributed to the neutral charge of HA. This value is within the range considered ideal for the circulation of nanomaterials in the bloodstream, because a neutral surface charge (±10 mV) can result in extended blood circulation times and lower the interaction with the reticuloendothelial system [10,21,42]. The stability tests indicate that the incubation in acidic pH and consequent protonation of the amines on PEI results in a slight increase in the AuMSS/PEI/HA nanoparticles' surface charge (Figure 2C & D). However, their negative surface charge and its maintenance during the 26 h of incubation further support the stability of the AuMSS nanorods functionalization with PEI and HA. The AuMSS functionalization was further confirmed by TGA analysis. The AuMSS nanorods' weight loss (5%) can be attributed to the evaporation of water adsorbed in the mesopores or to the loss of the hydroxyl groups at the external surface of AuMSS nanorods, whereas the AuMSS/PEI and AuMSS/PEI/HA weight curves can be attributed to the PEI and HA pyrolysis (Figure 1D). Additionally, the similarity between the TGA curve profiles of PEI and AuMSS/PEI indicate that the nanoparticles' weight loss is related to the PEI degradation. After confirming that AuMSS/PEI/HA nanorods possess the desirable physicochemical properties for cancer therapy, the photothermal capacity of AuMSS nanoparticles was evaluated. Both formulations presented the longitudinal and transversal resonance bands characteristics of gold nanorods (Figure 3A). Furthermore, the peak at 750 nm (i.e., NIR region) is consistent with the AR of gold nanorods (3.1), which also supports the applicability of these nanomaterials to mediate a photothermal effect. Upon NIR-laser irradiation, both formulations can mediate a temperature increase of ∼30°C, which indicates that the PEI-HA functionalization does not have a negative influence on the photothermal performance of the AuMSS-based nanomaterials (Figure 3B). Altogether, these results reveal that the AuMSS-based nanomaterials can mediate a temperature increase to values >42°C, which in the human body can lead to cells' destruction or increase their sensitivity to the chemotherapeutic action [6]. Drug encapsulation studies indicate that AuMSS nanorods functionalization led to an improved AO encapsulation efficiency and a slower and controlled AO release profile (Figure 4). These results can be attributed to the PEI and HA polymers that act as a barrier that difficult the AO diffusion and release from the silica mesopores. Different studies have shown that the coating of mesoporous silica with polymers can control the release of therapeutic agents loaded in the pores. For example, Moreira *et al.* reported that the AuMSS nanorods functionalization with poly-2-ethyl-2-oxazolines results in a slower and controlled doxorubicin release, 30% in 48 h contrasting with the 50% obtained to uncoated nanomaterials.

Additionally, Sun *et al.* observed that the grafting of PEI and folic acid on mesoporous silica nanoparticles prevented the curcumin release from silica pores at pH 7.4. However, when nanoparticles were incubated at pH 5.4, ~50% of the drug was released [43]. Otherwise, considering the potent photothermal property of the AuMSS-based materials, an increase in the drug release profile is also expected due to the increase in the drug's solubility, as previously reported in the literature [12,44].

The biocompatibility of AuMSS-based nanomaterials was evaluated by accessing the cytocompatibility and hemocompatibility of nanoparticles. Both AuMSS and AuMSS/PEI/HA showed excellent cytocompatibility in all tested concentrations (25–200 μg/ml) (Figure 5). These results demonstrate the safety of the AuMSS nanorods functionalization with PEI-HA and are in accordance with that reported in the literature for AuMSS nanoparticles [17]. Moreover, HA complexation in the PEI's surface also avoids the cytotoxicity often associated with the high positive charge density of the PEI chains [24,30,45]. Rodrigues *et al.* used different ratios of PEI to functionalize the D-α tocopherol polyethylene glycol 1000 succinate (TPGS) AuMSS nanoparticles [24]. The authors reported that the high PEI content on Au-MSS/TPGS/PEI (1:1) nanoparticles (formulation with a higher PEI content) affected the viability of HeLa cells; cells' viability decreased from ~80% to 40% with the increase of the concentration from 100 μg/ml to 200 μg/ml. The authors also described that the decrease of the PEI content from 1:1 to 3:1 led to better cytocompatibility results.

Despite the cytocompatibility, the AuMSS nanoformulations incubated with RBCs induce a concentration and time-dependent hemolysis, particularly for AuMSS and AuMSS/PEI nanomaterials (Figure 6 & Supplementary Figure 6). In the case of AuMSS/PEI nanoformulations, the increased hemolysis can be attributed to the highly positive surface charge of AuMSS/PEI nanomaterials (44 mV), which can lead to cell membrane' destabilization and cellular necrosis. The complexation of HA with the AuMSS/PEI nanomaterials masked this effect, improving nanoparticles' hemocompatibility. This increased safety of AuMSS/PEI/HA nanomaterials can be explained by the neutralization of the surface charge (-10 mV), which decreases interaction with the RBC membrane. Overall, these results are in accordance with previous reports of AuMSS nanomedicines as well as with the guidelines established by international agencies of the critically safe hemolytic ratio (ISO/TR 7406) [12,23,25].

Considering the HA affinity toward CD44, the HA complexation at the AuMSS/PEI nanorods' surface can confer an increased specificity to the nanomaterials toward cancer cells. Cellular internalization studies indicate that the PEI-HA functionalization enhances the AuMSS uptake, showing a preferential accumulation in the HeLa cells (i.e., a cell line that overexpresses the CD44) (Figure 7). Additionally, the two-fold decrease in the AuMSS/PEI/HA nanomaterials' uptake by HeLa cells after pretreatment with free HA further revealed the importance of the HA–CD44 interaction. This targeting capacity of the AuMSS/PEI/HA nanomaterials can lead to higher therapeutic performance by increasing the AO dose that reaches the cancer cells and reducing side effects in healthy tissues. Finally, the chemo-photothermal potential of AuMSS-based nanomaterials was assessed on HeLa cancer cells. The results demonstrate that the therapeutic combination (i.e., AO delivery and photothermal effect) potentiated the treatment effectiveness of both AuMSS and AuMSS/PEI/HA nanomaterials (Figure 8 & Supplementary Figure 7) leading to almost complete elimination of HeLa cells. These results are congruent with the photothermal data, where AuMSS-based nanomaterials induced a temperature increase of ~30°C. This temperature increment can directly promote the death of the HeLa cells and/or sensitize the cells for the AO action. The advantage of the PEI-HA functionalization was noted with standalone chemotherapy or PTT, where the HeLa cells presented significantly lower viability than those treated with AuMSS nanorods. This is attributed to the HA active targeting toward HeLa cancer cells, which increases cellular uptake and consequently improves therapeutic efficacy. Additionally, in the live/dead assays, the AuMSS/PEI/HA_AO-treated group showed a zone with dead cells that exceeded the NIR laser-irradiated area, that can be attributed to the enhanced therapeutic efficacy of the PTT-AO combination. Overall, these results confirm the NIR light activation of the photothermal therapeutic effect, which is indicative of the capacity to confine cytotoxic action to the irradiated cancer tissue. Moreover, beyond the potential of these nanomedicines in cancer therapy (e.g., chemotherapy and PTT), gold-core characteristic x-ray attenuation and surface-enhanced Raman scattering also support the applicability in biomedical imaging (e.g., computed tomographic, photoacoustic and thermal imaging) [46,47]. Additionally, the conjugation of multiple therapeutic modalities such as PTT, chemotherapy, immunotherapy and radiotherapy may also be achieved, making the AuMSS/PEI/HA a multifunctional nanomedicine [48,49].

Conclusion

AuMSS nanorods are multifunctional nanomedicines that can act simultaneously as photothermal, drug delivery and bioimaging agents. Nevertheless, when cancer therapy applications are intended, it is crucial to improve the nanoparticles' blood circulation time, stability, drug release profile and specificity toward cancer cells. With that in mind, in this study, PEI and HA were applied for the first time to functionalize AO-loaded AuMSS nanorods, creating a tumor-targeted chemo-photothermal nanomedicine.

The results demonstrate that the AuMSS nanorods functionalization did not affect its photothermal capacity. However, the HA functionalization promoted neutralization of AuMSS surface charge (from 44 to -10 mV) and consequently improved the biocompatibility of AuMSS by decreasing the blood hemolysis to safe levels. Additionally, the inclusion of PEI and HA on the AuMSS surface promoted a controlled and sustained AO release. *In vitro* assays performed in the 2D cell culture models demonstrated that the HA functionalization increased the nanoparticles' internalization by the HeLa cancer cells through a process mediated by the overexpressed CD44 receptors. Finally, the combinatorial treatment (i.e., chemotherapy and PTT) mediated by AuMSS/PEI/HA_AO nanorods presented an enhanced effect compared with the single PTT or chemotherapy regiments, leading to almost complete elimination of the cancer cells. Overall, these results confirm that AuMSS/PEI/HA_AO formulations can act as tumor-targeted chemo-photothermal nanomedicines for the combinatorial therapy of cervical cancer.

Future perspective

The application of NIR light-responsive nanomaterials – particularly AuMSS nanorods – is a hot topic, with several studies reporting their applicability in cancer chemo-photothermal therapy. However, the application of AuMSS nanorods as effective cancer nanomedicines is hindered by the uncontrolled drug release of the therapeutic agents, unfavorable pharmacokinetics profile, reduced tumor accumulation and lack of specificity toward cancer cells. Therefore, different strategies have been adopted to produce nanoparticles with better surface properties to improve their therapeutic performance and mediate a tumor-specific and spatial controlled cancer treatment. In the near future, the investigation and development of biomimetic (e.g., cell membrane camouflaged nanomaterials) or zwitterionic coatings, novel materials responsive to different stimuli (e.g., pH, redox, ROS) and the simultaneous conjugation with other therapeutic modalities (e.g., immunotherapy) will offer a personalized and more effective cancer treatment that may revolutionize cancer therapy.

Summary points

- Tumor-targeted chemo-photothermal therapy mediated by acridine orange (AO)-loaded gold-core silica shell (AuMSS) nanorods coated with polyethylenimine (PEI) and hyaluronic acid (HA) was studied.
- AuMSS nanorods functionalization was achieved through chemical linkage of a PEI–silane derivative followed by electrostatic adsorption of HA.
- The PEI and HA functionalized AuMSS nanorods (AuMSS/PEI/HA) presented superior AO loading and induced a controlled and sustained drug release.
- HA functionalization promoted the neutralization of the AuMSS' surface charge (44 to -10 mV) and improved AuMSS/PEI/HA nanorods' hemocompatibility.
- The AuMSS nanoformulations mediated a temperature increase of ~30°C through the near-infrared (NIR) laser irradiation.
- AuMSS/PEI/HA nanoparticles presented an increased cellular internalization in a process mediated by the overexpressed CD44 receptors.
- The chemo-photothermal combinatorial therapy enhanced the therapeutic efficacy against cervical cancer cells.

Supplementary data

To view the supplementary data that accompany this paper please visit the journal website at: www.futuremedicine.com/doi/suppl/10.2217/nnm-2021-0270

Author contributions

CF Rodrigues and AF Moreira contributed to the conceptualization of the study. CF Rodrigues, P Ferreira and AF Moreira contributed to the investigation of the study. CF Rodrigues contributed to the methodology and formal analysis of the study. N Fernandes contributed to the study's revisions and writing of the revised manuscript. CF Rodrigues, AF Moreira and D de Melo-Diogo were involved in the writing of the original draft and revised manuscript of this study. AF Moreira and IJ Correia supervised the study and contributed to the editing of the written draft.

Financial & competing interests disclosure

This work was financed by the Foundation for Science and Technology (FCT), through funds from the State Budget and by the European Regional Development Fund (ERDF), under the Portugal 2020 Program, through the Regional Operational Program of the Center (Centro2020), through the Project with the reference UIDB/00709/2020. The funding from CENTRO-01-0145-FEDER-028989 and POCI-01-0145-FEDER-031462 are also acknowledged. CF Rodrigues acknowledges a PhD fellowship from FCT (SFRH/BD/144680/2019). D de Melo-Diogo acknowledges CENTRO-01-0145-FEDER-028989 for the funding provided in the form of a research contract. The authors have no other relevant affiliations or financial involvement with any organization or entity with a financial interest in or financial conflict with the subject matter or materials discussed in the manuscript apart from those disclosed.

No writing assistance was utilized in the production of this manuscript.

References

Papers of special note have been highlighted as: • of interest; •• of considerable interest

1. Holohan C, Van Schaeybroeck S, Longley DB, Johnston PG. Cancer drug resistance: an evolving paradigm. *Nat. Rev. Cancer* 13(10), 714–726 (2013).
2. Al-Lazikani B, Banerji U, Workman P. Combinatorial drug therapy for cancer in the post-genomic era. *Nat. Biotechnol.* 30(7), 679–692 (2012).
3. Shrestha B, Tang L, Romero G. Nanoparticles-mediated combination therapies for cancer treatment. *Adv. Ther.* 2(11), 1900076 (2019).

•• **Combinatorial therapy mediated by nanomedicines for cancer therapy.**

4. Nam J, Son S, Ochyl LJ *et al*. Chemo-photothermal therapy combination elicits anti-tumor immunity against advanced metastatic cancer. *Nat. Commun.* 9(1), 1–13 (2018).
5. Wang X, Zhang J, Wang Y *et al.* Multi-responsive photothermal-chemotherapy with drug-loaded melanin-like nanoparticles for synergetic tumor ablation. *Biomaterials* 81, 114–124 (2016).
6. Chu KF, Dupuy DE. Thermal ablation of tumours: biological mechanisms and advances in therapy. *Nat. Rev. Cancer* 14(3), 199–208 (2014).
7. Kang JK, Kim JC, Shin Y *et al.* Principles and applications of nanomaterial-based hyperthermia in cancer therapy. *Arch. Pharmacal. Res.* 43(1), 46–57 (2020).
8. Fernandes N, Rodrigues CF, Moreira AF, Correia IJ. Overview of the application of inorganic nanomaterials in cancer photothermal therapy. *Biomater. Sci.* 8(11), 2990–3020 (2020).
9. Sharma S, Shrivastava N, Rossi F, Thanh NTK. Nanoparticles-based magnetic and photo induced hyperthermia for cancer treatment. *Nano Today* 29, 100795 (2019).
10. De Melo-Diogo D, Pais-Silva C, Dias DR *et al*. Strategies to improve cancer photothermal therapy mediated by nanomaterials. *Adv. Healthc. Mater.* 6(10), 1700073 (2017).
11. Tu X, Wang L, Cao Y *et al.* Efficient cancer ablation by combined photothermal and enhanced chemo-therapy based on carbon nanoparticles/doxorubicin@ SiO_2 nanocomposites. *Carbon* 97, 35–44 (2016).
12. Moreira AF, Rodrigues CF, Reis CA *et al*. Development of poly-2-ethyl-2-oxazoline coated gold-core silica shell nanorods for cancer chemo-photothermal therapy. *Nanomedicine* 13(20), 2611–2627 (2018).
13. Alves CG, De Melo-Diogo D, Lima-Sousa R *et al*. Hyaluronic acid functionalized nanoparticles loaded with IR780 and DOX for cancer chemo-photothermal therapy. *Eur. J. Pharm. Biopharm.* 137, 86–94 (2019).
14. Gonçalves AS, Rodrigues CF, Moreira AF, Correia IJ. Strategies to improve the photothermal capacity of gold-based nanomedicines. *Acta Biomater.* 16, 105–137 (2020).

•• **Summarizes the strategies to improve photothermal therapy of gold-based nanomaterials in cancer therapy.**

15. De Melo-Diogo D, Lima-Sousa R, Alves CG, Correia IJ. Graphene family nanomaterials for application in cancer combination photothermal therapy. *Biomater. Sci.* 7(9), 3534–3551 (2019).
16. Liu J, Liang H, Li M *et al.* Tumor acidity activating multifunctional nanoplatform for NIR-mediated multiple enhanced photodynamic and photothermal tumor therapy. *Biomaterials* 157, 107–124 (2018).
17. Moreira AF, Rodrigues CF, Reis CA *et al*. Gold-core silica shell nanoparticles application in imaging and therapy: a review. *Microporous Mesoporous Mater.* 270, 168–179 (2018).

•• **Application of gold-core mesoporous silica shell (AuMSS) nanomaterials in imaging and therapy.**

18. Kennedy LC, Bickford LR, Lewinski NA *et al.* A new era for cancer treatment: gold-nanoparticle-mediated thermal therapies. *Small* 7(2), 169–183 (2011).
19. Huang X, El-Sayed MA. Gold nanoparticles: optical properties and implementations in cancer diagnosis and photothermal therapy. *J. Adv. Res.* 1(1), 13–28 (2010).

20. Zhou Y, Quan G, Wu Q *et al.* Mesoporous silica nanoparticles for drug and gene delivery. *Acta Pharm. Sin. B.* 8(2), 165–177 (2018).
21. Rodrigues CF, Jacinto TA, Moreira AF *et al*. Functionalization of AuMSS nanorods towards more effective cancer therapies. *Nano Res.* 12(4), 719–732 (2019).
22. Zhang Y, Li M, Gao X *et al*. Nanotechnology in cancer diagnosis: progress, challenges and opportunities. *J. Hematol. Oncol.* 12(1), 1–13 (2019).
23. Reis CA, Rodrigues CF, Moreira AF *et al*. Development of gold-core silica shell nanospheres coated with poly-2-ethyl-oxazoline and β-cyclodextrin aimed for cancer therapy. *Mater. Sci. Eng. C* 98, 960–968 (2019).
24. Rodrigues CF, Reis CA, Moreira AF *et al*. Optimization of gold core-mesoporous silica shell functionalization with TPGS and PEI for cancer therapy. *Microporous Mesoporous Mater.* 285, 1–12 (2019).

- **Improved biological performance of PEI/TPGS functionalized AuMSS nanorods for cancer therapy.**

25. Jacinto TA, Rodrigues CF, Moreira AF *et al.* Hyaluronic acid and vitamin E polyethylene glycol succinate functionalized gold-core silica shell nanorods for cancer targeted photothermal therapy. *Colloids Surf. B* 188, 110778 (2020).

- **Improved photothermal therapy and biological performance of hyaluronic acid functionalized AuMSS nanorods for cancer-targeted photothermal therapy.**

26. Byvaltsev VA, Bardonova LA, Onaka NR *et al.* Acridine orange: a review of novel applications for surgical cancer imaging and therapy. *Front. Oncol.* 9, 925 (2019).
27. Guimarães RS, Rodrigues CF, Fernandes N *et al.* Combinatorial delivery of doxorubicin and acridine orange by gold core silica shell nanospheres functionalized with poly(ethylene glycol) and 4-methoxybenzamide for cancer targeted therapy. *J. Inorg. Biochem.* 219, 111433 (2021).
28. Bragagni M, Carta F, Osman SM *et al*. Synthesis of an acridine orange sulfonamide derivative with potent carbonic anhydrase IX inhibitory action. *J. Enzyme Inhib. Med. Chem.* 32(1), 701–706 (2017).
29. Iessi E, Logozzi M, Lugini L *et al.* Acridine orange/exosomes increase the delivery and the effectiveness of acridine orange in human melanoma cells: a new prototype for theranostics of tumors. *J. Enzyme Inhib. Med. Chem.* 32(1), 648–657 (2017).
30. Zakeri A, Kouhbanani MaJ, Beheshtkhoo N *et al.* Polyethylenimine-based nanocarriers in co-delivery of drug and gene: a developing horizon. *Nano Rev. Exp.* 9(1), 1488497 (2018).
31. Vermeulen LM, De Smedt SC, Remaut K, Braeckmans K. The proton sponge hypothesis: fable or fact? *Eur. J. Pharm. Biopharm.* 129, 184–190 (2018).
32. Amorim S, Da Costa DS, Freitas D *et al.* Molecular weight of surface immobilized hyaluronic acid influences CD44-mediated binding of gastric cancer cells. *Sci. Rep.* 8(1), 1–11 (2018).
33. Lee SY, Kang MS, Jeong WY *et al*. Hyaluronic acid-based theranostic nanomedicines for targeted cancer therapy. *Cancers* 12(4), 940 (2020).
34. Dias DR, Moreira AF, Correia IJ. The effect of the shape of gold core-mesoporous silica shell nanoparticles on the cellular behavior and tumor spheroid penetration. *J. Mater. Chem. B* 4(47), 7630–7640 (2016).
35. Moreira AF, Dias DR, Costa EC, Correia IJ. Thermo-and pH-responsive nano-in-micro particles for combinatorial drug delivery to cancer cells. *Eur. J. Pharm. Sci.* 104, 42–51 (2017).
36. Moreira AF, Gaspar VM, Costa EC *et al.* Preparation of end-capped pH-sensitive mesoporous silica nanocarriers for on-demand drug delivery. *Eur. J. Pharm. Biopharm.* 88(3), 1012–1025 (2014).
37. Gaspar VM, Moreira AF, Costa EC *et al.* Gas-generating TPGS-PLGA microspheres loaded with nanoparticles (NIMPS) for co-delivery of minicircle DNA and anti-tumoral drugs. *Colloids Surf. B* 134, 287–294 (2015).
38. Yu M, Jambhrunkar S, Thorn P *et al*. Hyaluronic acid modified mesoporous silica nanoparticles for targeted drug delivery to CD44-overexpressing cancer cells. *Nanoscale* 5(1), 178–183 (2013).
39. Becker J, Trügler A, Jakab A *et al*. The optimal aspect ratio of gold nanorods for plasmonic bio-sensing. *Plasmonics* 5(2), 161–167 (2010).
40. Wang S, Xi W, Cai F *et al.* Three-photon luminescence of gold nanorods and its applications for high contrast tissue and deep in vivo brain imaging. *Theranostics* 5(3), 251 (2015).
41. Cheng D, Ji Y, Wang B *et al.* Dual-responsive nanohybrid based on degradable silica-coated gold nanorods for triple-combination therapy for breast cancer. *Acta Biomater.* 128, 435–446 (2021).
42. Rodrigues CF, Alves CG, Lima-Sousa R, *et al*. Inorganic-based drug delivery systems for cancer therapy. In: *Advances and Avenues in the Development of Novel Carriers for Bioactives and Biological Agents.*Singh RW, Singh D, Kanwar JR, Chuhuan NS (Eds). Elsevier/Academic Press, London, UK, 283–316 (2020).
43. Sun X, Wang N, Yang L-Y *et al*. Folic acid and PEI modified mesoporous silica for targeted delivery of curcumin. *Pharmaceutics* 11(9), 430 (2019).
44. Song Z, Shi J, Zhang Z *et al*. Mesoporous silica-coated gold nanorods with a thermally responsive polymeric cap for near-infrared-activated drug delivery. *J. Mater. Sci.* 53(10), 7165–7179 (2018).

45. Monnery BD, Wright M, Cavill R *et al.* Cytotoxicity of polycations: relationship of molecular weight and the hydrolytic theory of the mechanism of toxicity. *Int. J. Pharm.* 521(1-2), 249–258 (2017).

46. Khademi S, Sarkar S, Kharrazi S *et al.* Evaluation of size, morphology, concentration, and surface effect of gold nanoparticles on x-ray attenuation in computed tomography. *Physica Medica* 45, 127–133 (2018).

47. Keshavarz M, Moloudi K, Paydar R *et al.* Alginate hydrogel co-loaded with cisplatin and gold nanoparticles for computed tomography image-guided chemotherapy. *J. Biomater. Appl.* 33(2), 161–169 (2018).

48. Mirrahimi M, Beik J, Mirrahimi M *et al.* Triple combination of heat, drug and radiation using alginate hydrogel co-loaded with gold nanoparticles and cisplatin for locally synergistic cancer therapy. *Int. J. Biol. Macromol.* 158, 617–626 (2020).

49. Mirrahimi M, Khateri M, Beik J *et al.* Enhancement of chemoradiation by co-incorporation of gold nanoparticles and cisplatin into alginate hydrogel. *J. Biomed. Mater. Res. Part B* 107(8), 2658–2663 (2019).